MEMS SoC: observer-based coplanar gyro-free inertial measurement unit

2005 J. Micromech. Microeng. 15 1664

(http://iopscience.iop.org/0960-1317/15/9/008)

INSTITUTE OF PHYSICS PUBLISHING JOURNAL OF MICROMECHANICS AND MICROENGINEERING

J. Micromech. Microeng. **15** (2005) 1664–1673 doi:10.1088/0960-1317/15/9/008

MEMS SoC: observer-based coplanar gyro-free inertial measurement unit

Tsung-Lin Chen[1] **and Sungsu Park**[2]

[1] Department of Mechanical Engineering, National Chiao Tung University, Shinchu, Taiwan, Republic of China

[2] Department of Aerospace Engineering, Sejong University, Seoul, Korea

E-mail: tsunglin@mail.nctu.edu.tw and sungsu@sejong.ac.kr

Received 25 February 2005, in final form 28 April 2005
Published 15 July 2005
Online at stacks.iop.org/JMM/15/1664

Abstract

This paper presents a novel design of a coplanar gyro-free inertial measurement unit (IMU) that consists of seven to nine single-axis linear accelerometers, and it can be utilized to perform the six DOF measurements for an object in motion. Unlike other gyro-fee IMUs, this design uses redundant accelerometers and state estimation techniques to facilitate the *in situ* and mass fabrication for the employed accelerometers. The alignment error from positioning accelerometers onto a measurement unit and the fabrication cost of an IMU can greatly be reduced. The outputs of the proposed design are three linear accelerations and three angular velocities. As compared to other gyro-free IMUs, the proposed design uses less integral operation and thus improves its sensing resolution and drifting problem. The sensing resolution of a gyro-free IMU depends on the sensing resolution of the employed accelerometers as well as the size of the measurement unit. Simulation results indicate that the sensing resolution of the proposed design is $2^\circ\ s^{-1}$ for the angular velocity and 10 μg for the linear acceleration when nine single-axis accelerometers, each with 10 μg sensing resolution, are deployed on a 4 inch diameter disc. Also, thanks to the iterative EKF algorithm, the angle estimation error is within 10^{-3} deg at 2 s.

(Some figures in this article are in colour only in the electronic version)

1. Introduction

An IMU (inertial measurement unit) is a sensor unit that performs the integrated measurement of the six DOF movement parameters. In this way, we can obtain the position of an object in motion in space, which includes: three location coordinates in X, Y, Z and three rotation angles in pitch, yaw and roll. As compared to other sensing techniques that perform six DOF measurements, an IMU has the advantages of mobility and thus has been widely utilized in navigation systems for precise positioning [1–3].

Most of the IMU systems consist of three gyroscopes and three linear accelerometers. And they acquire the orientation angles of an object in motion by one integral operation on the angular velocities, which are measurements from gyroscopes; the location information by two consecutive integral operations on the linear acceleration, which are measurements from linear accelerometers [1–4]. This approach is straightforward and can accurately acquire the six DOF movement parameters as long as the high precision inertial sensors are incorporated in the IMU. Due to the fact that high-precision gyroscopes are usually more expensive than accelerometers, some researchers proposed gyro-free IMU systems, which implies that the proposed six DOF measurement unit consists of accelerometers only [5–8]. As concluded in those reports, the sensing resolution of gyro-free IMUs is usually worse than IMUs composed of gyroscopes and accelerometers. However, gyro-free IMUs are inexpensive and thus applicable to lots of applications that require low-cost and medium performance, such as those for car navigation [9], virtual reality [10] etc.

In the conventional gyro-free IMU designs, accelerometers had to be attached to the object in motion at specific locations, in a 3D manner, to ensure its proper operation. As a consequence, it is not only expensive

to assemble but also susceptible to alignment error that would deteriorate its sensing resolution. The outputs of gyro-free IMUs for rotation dynamics can either be angular acceleration or angular velocity, depending on the configuration of accelerometers deployed in an IMU. Furthermore, the configuration that produces angular acceleration measurements is considered to be more reliable than that of angular velocity and thus has been widely adopted [5]. Since the outputs of most gyro-free IMUs are angular accelerations and linear accelerations, they need one more integral operation than the IMU composed of gyroscopes and accelerometers, which makes them more vulnerable in cases where dc bias and/or noise are present in accelerometers measurements [11].

In the past few years, MEMS (micro electro mechanical systems) research work focused on device physics and component-level designs and has made distinct MEMS inertial sensors affordable to lots of applications. Nowadays, research effort has gradually migrated from MEMS components design to MEMS systems design aiming for better system performance and more effective cost reduction. Above is the concept of MEMS SoC (system on chip) and has been considered as the next milestone in the MEMS research area. One of the major challenges in the MEMS SoC is the fabrication process integration for a variety of components in a system. Most of the MEMS process fabricated components on the same facet of a wafer, which hampers the possibility of fabricating a conventional gyro-free IMU as a MEMS SoC. In a word, for the gyro-free IMUs to benefit from the approaches of MEMS SoC, all the incorporated sensors must be *in situ* fabricated on the same substrate of a wafer.

In this paper, we proposed a brand new coplanar gyro-free IMU design. Our design used redundant accelerometers and state estimation techniques. As such, all the employed accelerometers can be situated on the same facet of the measurement unit and still have a stable operation. Furthermore, these incorporated accelerometers can be *in situ* and mass fabricated by some accelerometer-making processes. These unique features facilitated the concept of MEMS SoC and minimized the error and cost from positioning accelerometers onto the object to be measured. Moreover, the output of the proposed gyro-free IMU are three angular velocities and three linear accelerations. The integral operation is reduced by one and thus greatly improved the sensing resolution and drifting problem [11].

2. Gyroscope-free inertial measurement unit design

2.1. Gyroscope-free inertial measurement theory

Figure 1 shows the relation between the earth-centered inertial frame $\{i\}$ and body frame $\{b\}$. $\vec{R}_o$ is a position vector from earth-center to the center of the body frame. $\vec{R}_j$ is a position vector from earth-center to location j and $\vec{r}_j$ is a position vector from the center of the body frame to location j. $\vec{w}$ is the rotation rate of the body frame. According to the coordinate transformation, the acceleration at location j can be written as follows:

$$\ddot{\vec{R}}_j = \ddot{\vec{R}}_o + \dot{\vec{w}} \times \vec{r}_j + \vec{w} \times (\vec{w} \times \vec{r}_j) + 2\vec{w} \times \dot{\vec{r}}_j + \ddot{\vec{r}}_j. \quad (1)$$

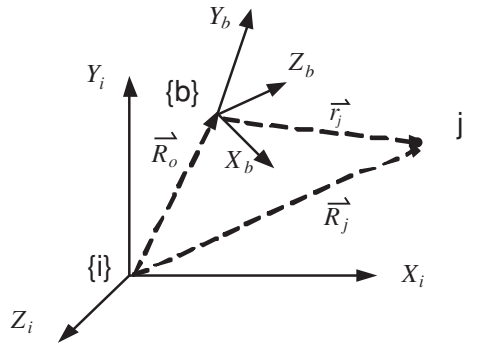

Figure 1. The schematic of inertial frame versus body frame.

In the case that the body frame is rotated with the object in motion, ${}^b r_j$, the $\vec{r}_j$ vector represented in the body frame, is constant. Therefore, equation (1) can be simplified as follows,

$$\begin{aligned} {}^i\ddot{R}_j &= {}^i\ddot{R}_o + C_b^{ib}\dot{w} \times {}^b r_j + C_b^{ib} w \times ({}^b w \times {}^r r_j) \\ {}^i\ddot{R}_j &= {}^i F_j + {}^i g, \end{aligned} \quad (2)$$

where ${}^i F_j$ is the specific force applied at location j and ${}^i g$ is the gravitational force, both of which are represented in the inertial frame. C_b^i is the conversion matrix that can transform a vector represented in the body frame into a vector represented in the inertial frame. Assuming (1) a single-axis accelerometer is rigidly mounted on the object at the location j with the sensing direction of $\vec{\eta}_j$ and (2) the gravitational force can be obtained in advance and the accelerometer output is calibrated such that it responds to the specific force only, the accelerometer output A_j can be written in the following:

$$\begin{aligned} A_j &= \ddot{\vec{R}}_j \cdot \vec{\eta}_j = {}^b\ddot{R}_j \cdot {}^b\eta_j \\ &= C_b^i\left({}^i F_o + C_i^{bb}\dot{w} \times {}^b r_j + C_i^{bb} w({}^b w \times {}^b r_j)\right) \cdot {}^b\eta_j \\ &= [({}^b r_j \times {}^b\eta_j)^T \, {}^b\eta_j] \begin{bmatrix} {}^b\dot{w} \\ {}^b F_o \end{bmatrix} + {}^b\eta_j^T \cdot ({}^b w \times ({}^b w \times {}^b r_j)). \end{aligned} \quad (3)$$

Supposing there are m accelerometers distributed onto the object, the accelerometers measurements can be arranged in vector form,

$$\begin{bmatrix} A_1 \\ \vdots \\ A_j \\ \vdots \\ A_m \end{bmatrix} = J \cdot \begin{bmatrix} {}^b\dot{w} \\ {}^b F_o \end{bmatrix} + \begin{bmatrix} {}^b\eta_1^T \cdot ({}^b w \times ({}^b w \times {}^b r_1)) \\ \vdots \\ {}^b\eta_j^T \cdot ({}^b w \times ({}^b w \times {}^b r_j)) \\ \vdots \\ {}^b\eta_m^T \cdot ({}^b w \times ({}^b w \times {}^b r_m)) \end{bmatrix}$$

$$J = \begin{bmatrix} ({}^b r_1 \times {}^b\eta_1)^T & {}^b\eta_1 \\ \vdots & \\ ({}^b r_j \times {}^b\eta_j)^T & {}^b\eta_j \\ \vdots & \\ ({}^b r_m \times {}^b\eta_m)^T & {}^b\eta_m \end{bmatrix}. \quad (4)$$

If the matrix $J^T J$ is invertible, the relation between the dynamics of an object in motion and the measurements from accelerometers located at various locations can be shown

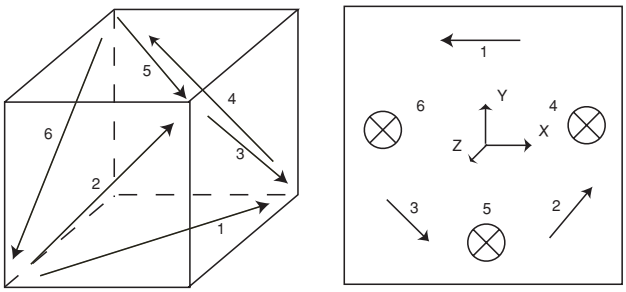

Figure 2. Cube-type gyro-free IMU versus coplanar gyro-free IMU. The arrows denote the sensing direction of each accelerometer.

as follows:

$$\begin{bmatrix} {}^b\dot{w} \\ {}^bF_o \end{bmatrix}_{6\times 1} = (J^TJ)^{-1}J^T\left(\begin{bmatrix} A_1 \\ \vdots \\ A_j \\ \vdots \\ A_m \end{bmatrix} - \begin{bmatrix} {}^b\eta_1^T\cdot({}^bw\times({}^bw\times{}^br_1)) \\ \vdots \\ {}^b\eta_j^T\cdot({}^bw\times({}^bw\times{}^br_j)) \\ \vdots \\ {}^b\eta_m^T\cdot({}^bw\times({}^bw\times{}^br_m)) \end{bmatrix}\right). \tag{5}$$

Excerpting from equation (5), we obtain a set of nonlinear differential equations for the angular velocity.

$$[{}^b\dot{w}]_{3\times 1} = (J^TJ)^{-1}J^T(1:3,:) \times\left(\begin{bmatrix} A_1 \\ \vdots \\ A_j \\ \vdots \\ A_m \end{bmatrix} - \begin{bmatrix} {}^b\eta_1^T\cdot({}^bw\times({}^bw\times{}^br_1)) \\ \vdots \\ {}^b\eta_j^T\cdot({}^bw\times({}^bw\times{}^br_j)) \\ \vdots \\ {}^b\eta_m^T\cdot({}^bw\times({}^bw\times{}^br_m)) \end{bmatrix}\right). \tag{6}$$

Equation (6) is referred to as the 'governing equation' in this report.

According to the governing equation, for the existence of the $(J^TJ)^{-1}$, the minimum number of accelerometers needed for a gyro-free IMU is six. Furthermore, the complexity and nonlinearity of the governing equation depend on the locations and sensing directions of accelerometers deployed onto the object. Most of the in-use gyro-free IMU designs use the configuration of accelerometers deployment shown in figure 2 [6–8], for the reason that the associated nonlinear terms in equation (6) disappeared. Those IMU designs obtain angular accelerations by sum/subtraction on accelerometer measurements and result in a stable and reliable operation. However, the expense is that it needs two consecutive integration operations to obtain orientation angles.

2.2. Planar-type gyro-free IMU

The proposed coplanar configuration denotes that all the accelerometers employed in the measurement unit are situated on the same facet of the measurement unit at the same elevation. The way to construct such a gyro-free IMU, using the minimum number of accelerometers, is employing three accelerometers measuring the acceleration along the direction parallel to the plane surface of the measurement unit (in-plane sensing), and the other three accelerometers measuring the acceleration along the direction perpendicular to the plane surface of the measurement unit (out-of-plane sensing). This is because the in-plane sensing accelerometers can provide, at most, three linearly independent row vectors for the J matrix, and out-of-plane sensing accelerometers can provide, at most, another three linearly independent row vectors for the J matrix. These six single-axis accelerometers, employed for constructing an invertible J matrix, are referred to as 'system-accelerometers' in this paper. Figure 2 shows an example of the proposed coplanar gyro-free IMU design. The biggest advantage of the coplanar configuration is that all the accelerometers can be *in situ* fabricated on the same substrate at the same time and thus the fabrication cost and alignment error are minimized. However, the shortcoming is that the resulting governing equation is nonlinear.

2.3. Observer-based gyro-free IMU

After acquiring the governing equation, the operation of a gyro-free IMU is indeed an 'observer' problem, meaning that obtaining system states information, angular velocities of a physical system in this case, with the knowledge of the system governing equation. According to the observability theories [12], we can only implement an 'open-loop observer' for this system because there is no 'system output' associated with the governing equation. Furthermore, an open-loop observer can observe system states successfully only when either the system is stable or the knowledge of initial conditions is presumed. In the coplanar gyro-free IMU design, it can be shown that (appendix A) the stability of the system depends on the angular velocities to be measured, and no matter what the accelerometers configuration is, the system would become unstable along with the trajectory of angular velocity. As suggested by the observability theories, we would implement a 'closed-loop observer' to solve the open-loop observer problem, and firstly is to find the 'output' for the system.

We proposed using redundant accelerometers, other than the previously described system-accelerometers, to create outputs for the system. These accelerometers are referred to as 'observer-accelerometers' in this paper. Since they are accelerometers deployed in the IMU, these observer-accelerometers can be described by equation (3). Furthermore, these observer-accelerometers outputs can be arranged in a way to associate themselves with the outputs from system-accelerometers. As a result, the observer-accelerometer output consists of measurements from system-accelerometers and angular velocities only.

$$\begin{bmatrix} A_{o1} \\ \vdots \\ A_{oj} \\ \vdots \\ A_{om} \end{bmatrix} = \begin{bmatrix} ({}^br_{o1}\times{}^b\eta_{o1})^T & {}^b\eta_{o1} \\ \vdots & \\ ({}^br_{oj}\times{}^b\eta_{oj})^T & {}^b\eta_{oj} \\ \vdots & \\ ({}^br_{om}\times{}^b\eta_{om})^T & {}^b\eta_{om} \end{bmatrix}(J^TJ)^{-1}J^T \times\left(\begin{bmatrix} A_1 \\ \vdots \\ A_j \\ \vdots \\ A_m \end{bmatrix} - \begin{bmatrix} {}^b\eta_1^T\cdot({}^bw\times({}^bw\times{}^br_1)) \\ \vdots \\ {}^b\eta_j^T\cdot({}^bw\times({}^bw\times{}^br_j)) \\ \vdots \\ {}^b\eta_m^T\cdot({}^bw\times({}^bw\times{}^br_m)) \end{bmatrix}\right)$$

$$+\begin{bmatrix} {}^{b}\eta_{o1}^{T}\cdot({}^{b}w\times({}^{b}w\times{}^{b}r_{o1})) \\ \vdots \\ {}^{b}\eta_{oj}^{T}\cdot({}^{b}w\times({}^{b}w\times{}^{b}r_{oj})) \\ \vdots \\ {}^{b}\eta_{om}^{T}\cdot({}^{b}w\times({}^{b}w\times{}^{b}r_{om})) \end{bmatrix}. \tag{7}$$

Equation (7) can be treated as system outputs for a gyro-free IMU system. Combining governing equation (6) and system output (7), we now have enough information to construct a closed-loop observer to identify angular velocities.

A legitimate question to ask is: where these observer-accelerometers should be located, most importantly, what the sensing directions of these accelerometers should be? A simple derivation (appendix B) shows that any out-of-plane sensing accelerometer, other than those in system-accelerometers, cannot provide angular velocity information in equation (7). Therefore, the observer-accelerometers must be in-plane sensing accelerometers.

In a dynamic system, the rank of an observability matrix and its associated singular values are the indications for the feasibility of an observer design [13]. The observability matrix of a nonlinear system can be obtained as follows:

$$W_o = \nabla[z\dot{z}\ldots]', \qquad z = [A_{o1}\ldots A_{oj}\ldots A_{om}]. \tag{8}$$

In this particular case, the existence of derivatives of z depends on the derivatives of angular velocity. Consequently, the number of row vectors in the observability matrix is determined by the existence of high-order derivatives of angular velocity along the trajectory.

As shown in equations (7) and (8), the configuration of system-accelerometers and observer-accelerometers affects the observability of a system and thus the performance of states estimation speed and accuracy. Even though we know, in theory, we should design the accelerometer configuration (number of incorporated accelerometers, locations, sensing directions, etc) based on the system observability matrix, it is extremely difficult to do so not only because the analytical solution of the observability matrix is complicated but also the observability of a nonlinear system depends on the angular velocities to be measured. For those reasons, the observer-accelerometers design is chosen to cope with one extreme case in which the angular velocities to be measured are constant. In that case, equation (6) becomes static and we need to have three outputs to ensure the rank of the observability matrix of three mostly. Therefore, we determined the number of observer-accelerometers is three.

3. Data processing

3.1. Noise channel

To mimic the real device in use and to determine the sensing resolution for the gyro-free IMU, we implemented noise signals along with each accelerometer measurement in simulation. To be able to construct an observer for a system contaminated by noise, the noise term is retrofit into the governing equation and output equation, as shown in equation (9). The covariance of noise in the governing equation and output equation can be obtained accordingly.

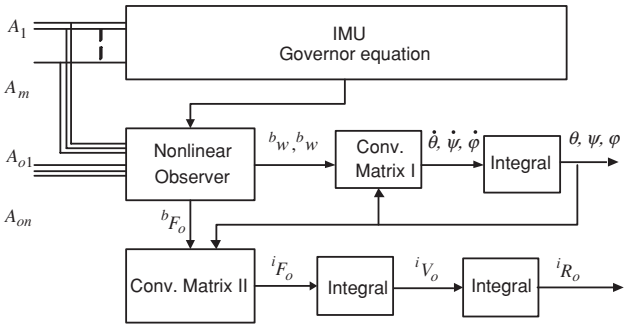

Figure 3. Data processing flow chart for coplanar gyro-free IMU.

$$\begin{bmatrix} \dot{w}_1 \\ \dot{w}_2 \\ \dot{w}_3 \end{bmatrix} = J^{-1}(1:3,:)\left(\begin{bmatrix} \vdots \\ w \quad \text{terms} \\ \vdots \end{bmatrix} + \begin{bmatrix} A_1 \\ \vdots \\ A_6 \end{bmatrix} + \begin{bmatrix} n_{A_1} \\ \vdots \\ n_{A_6} \end{bmatrix}\right)$$
$$\begin{bmatrix} A_{o1} \\ A_{o2} \\ A_{o3} \end{bmatrix} = J\cdot\begin{bmatrix} {}^{b}\dot{w} \\ {}^{b}F_o \end{bmatrix} + \begin{bmatrix} {}^{b}\eta_{o1}^{T}\cdot({}^{b}w\times({}^{b}w\times{}^{b}r_{o1})) \\ {}^{b}\eta_{o2}^{T}\cdot({}^{b}w\times({}^{b}w\times{}^{b}r_{o2})) \\ {}^{b}\eta_{o3}^{T}\cdot({}^{b}w\times({}^{b}w\times{}^{b}r_{o3})) \end{bmatrix} + \begin{bmatrix} n_{A_7} \\ n_{A_8} \\ n_{A_9} \end{bmatrix}. \tag{9}$$

3.2. Nonlinear observers

A suitable closed-loop observer, an observer that can work with a nonlinear system, is chosen for the subsequent data processing. There are several nonlinear observer methods available including: extended Kalman filter, Thau's approach, sliding observers, linearizable error dynamics, adaptive observers, etc [14–16]. Most of those methods rely on a nonlinear transformation to set up new system states for the ease of subsequent data processing [15]. These approaches are not applicable to our case since the nonlinear terms in equations (6) and (7) are all of second order and it would encounter sign problems during the nonlinear transformation. In addition to that, the states noise contamination could be amplified due to the nonlinear transformation. For that reason, we chose the extended Kalman filter (EKF) method. The EKF method is effective at noise reduction but it cannot guarantee the convergence of state estimation even with the complicated first- or second-order EKF method [17]. Finally, the iterative EKF method is utilized to achieve both noise reduction and states convergence.

3.3. Block diagram

Figure 3 shows the block diagram of the data processing for our observer-based IMU design. As shown in the diagram, both the angular velocity (${}^{b}w$) and the force (${}^{b}F_o$) represented in the body frame are obtained by choosing a proper nonlinear observer. The ${}^{b}w$ is first converted to the angular velocity along with the direction of Euler angles for the track of Euler angles. The Euler angles are then utilized to convert the dynamics information represented in the body frame into the inertial frame.

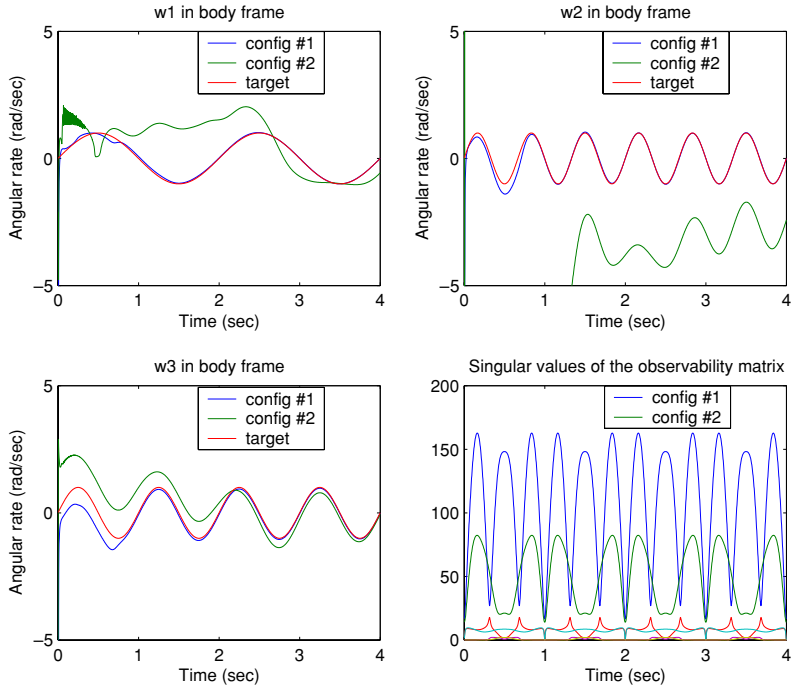

Figure 4. States trajectories versus observability matrix for different configurations.

4. Results and discussions

4.1. States convergence versus observability matrix

Here, we show two design examples to illuminate the connections between the observability matrix and states estimation. These two designs both have seven accelerometers (six system-accelerometers and one observer-accelerometer), but they have different accelerometers configurations. The first system has the following state equations,

$$\begin{bmatrix} \dot{w}_1 \\ \dot{w}_2 \\ \dot{w}_3 \end{bmatrix} = C_1 \cdot \begin{bmatrix} A_1 \\ \vdots \\ A_6 \end{bmatrix} + \begin{bmatrix} w_2 w_3 \\ -w_1 w_3 \\ 0.39w_1^2 + 0.31w_2^2 + 0.7w_3^2 + 0.2w_1 w_2 \end{bmatrix}$$
$$A_7 = C_2 \cdot \begin{bmatrix} A_1 \\ \vdots \\ A_6 \end{bmatrix} + 1.08w_1^2 + 0.65w_2^2 + 1.73w_3^2 - 1.14w_1 w_2 \tag{10}$$

and the second system:

$$\begin{bmatrix} \dot{w}_1 \\ \dot{w}_2 \\ \dot{w}_3 \end{bmatrix} = C_3 \cdot \begin{bmatrix} A_1 \\ \vdots \\ A_6 \end{bmatrix} + \begin{bmatrix} w_2 w_3 \\ -w_1 w_3 \\ 0 \end{bmatrix}$$
$$A_7 = C_4 \cdot \begin{bmatrix} A_1 \\ \vdots \\ A_6 \end{bmatrix} - w_1^2 + w_3^2. \tag{11}$$

In this simulation, the trajectory to be followed is sinusoidal. Therefore, as discussed previously, the observability matrices of both systems do consist of infinite terms and the rank of matrices are expected to be three even though there is only one output in the system. For comparison purposes, we show the numerical simulations of the first three row vectors in the observability matrices in two systems along with states trajectory. As shown in figure 4, configuration 1 tracks the trajectory better than configuration 2, and the singular values of the observability matrix in the first case are larger than those in the second case. Although it shows a connection between observability matrix and state convergence in simulation, we have to point out that the magnitude of singular values is not explicitly related to the observing speed and accuracy. The principle of the iterative EKF method tries to minimize the noise variance and state estimation error iteratively. And its state estimation is done by the numerical search on possible states combinations that minimize the discrepancy between estimated output and measured output. Since there are three states associated with single output in the system, it cannot guarantee that the state estimation would converge toward the correct values in each state estimation phase.

4.2. A design example

Here we show a design example: the nine single-axis accelerometers are distributed on a 4 inch diameter disc to form a coplanar, gyro-free IMU. The location and sensing direction of each accelerometer are listed in table 1. Accelerometers 1–6 are system-accelerometers and accelerometers 7–9 are observer-accelerometers. The trajectories to be followed are: three constant Euler angle rotation rates, 28.8° s^{-1}, 36° s^{-1}, 43.2° s^{-1} and three linear accelerations of 100 μg, 150 μg, 200 μg in the inertial frame. The noise incorporated in the simulation is white noise, and without loss of generalities, the noise associated with each accelerometer measurement is assumed to have the same standard deviation of 10 μg. The signal-to-noise ratio is about 10. The nine accelerometer measurements along with the trajectory are shown in figure 5.

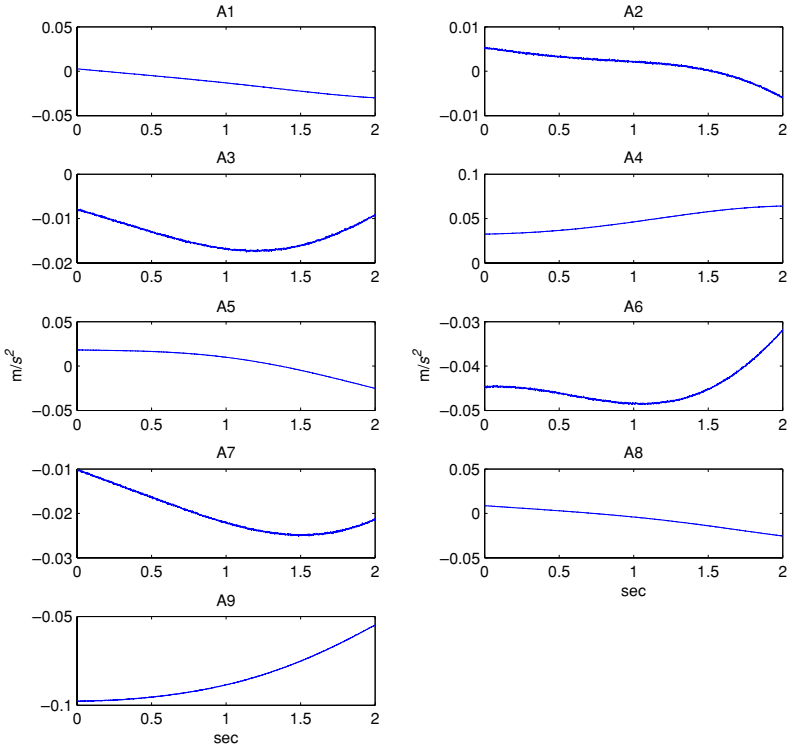

Figure 5. Nine single-axis accelerometer measurements along with the designated trajectory.

Table 1. Configuration of nine single-axis accelerometers.

Accelerometer number	Location ${}^b r_j(x, y, z)$	Sensing direction ${}^b \eta_j(x, y, z)$
1	$r[\cos(4\pi/9) \quad \sin(4\pi/9) \quad 0]$	$[\cos(17\pi/18) \quad \sin(17\pi/18) \quad 0]$
2	$r[\cos(10\pi/9) \quad \sin(10\pi/9) \quad 0]$	$[\cos(-7\pi/18) \quad \sin(-7\pi/18) \quad 0]$
3	$r[\cos(16\pi/9) \quad \sin(16\pi/9) \quad 0]$	$[\cos(5\pi/18) \quad \sin(5\pi/18) \quad 0]$
4	$r[\cos(2\pi/9) \quad \sin(2\pi/9) \quad 0]$	$[0 \quad 0 \quad 1]$
5	$r[\cos(8\pi/9) \quad \sin(8\pi/9) \quad 0]$	$[0 \quad 0 \quad 1]$
6	$r[\cos(14\pi/9) \quad \sin(14\pi/9) \quad 0]$	$[0 \quad 0 \quad 1]$
7	$r[\cos(6\pi/9) \quad \sin(6\pi/9) \quad 0]$	$[\cos(7\pi/6) \quad \sin(7\pi/6) \quad 0]$
8	$r[\cos(12\pi/9) \quad \sin(12\pi/9) \quad 0]$	$[\cos(-1\pi/6) \quad \sin(-1\pi/6) \quad 0]$
9	$r[1 \quad 0 \quad 0]$	$[1 \quad 0 \quad 0]$

Figure 6 shows the angular velocities represented in the body frame converge to their designated values. Thanks to the Kalman filter, the standard deviation of estimated angular velocities decreases along with the estimation time. The standard deviation of angular velocities reaches 5×10^{-5} rad s^{-1} after 2 s in simulation.

Figure 7 shows the linear accelerations represented in the body frame converge to their designated values although the output signals are noisy. The reason for this is that the calculation of linear accelerations uses measurements from accelerometers directly, and the noise associated with accelerometer measurements bypasses the Kalman filter. The standard deviations of a_1, a_2 are larger than that of a_3 and it is because the calculation of a_1, a_2 needs information of angular velocity, while a_3 does not. The calculation of a_3 uses measurements from three out-of-plane sensing accelerometers only. As a consequence, the standard deviation of a_3 corresponds to $(10\ \mu g)/\sqrt{3}$.

Figure 8 shows the convergence of Euler angles and their designated values. As shown in the lower right plot, the error accumulation due to pure integral operation is not noticeable and in fact, the error converges and diverges at different time segments. The first section of convergence is due to the fact that the EKF algorithm quickly corrects the mismatch in initial conditions. After that, the standard deviation of the angular velocities keeps decreasing with the help of the EKF algorithm. As a result, the error accumulation in orientation angles is concealed by the decrease of the standard deviation of angular velocities. The angle estimation error is of the order of 10^{-3} deg after 2 s of simulation.

Figure 9 shows angular velocities and linear accelerations, represented in the inertial frame, converge to their designated values.

4.3. Estimated sensing resolution

To find the sensing resolution of this IMU, we keep lowering the magnitude of designated angular velocities and linear accelerations while keeping the standard deviation of the

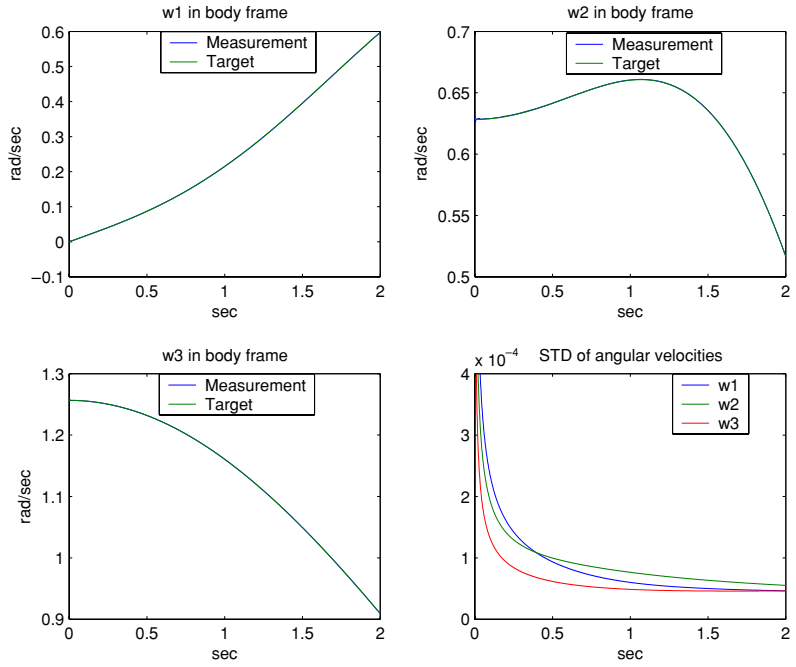

Figure 6. Angular velocities represented in the body frame converge to their designated values.

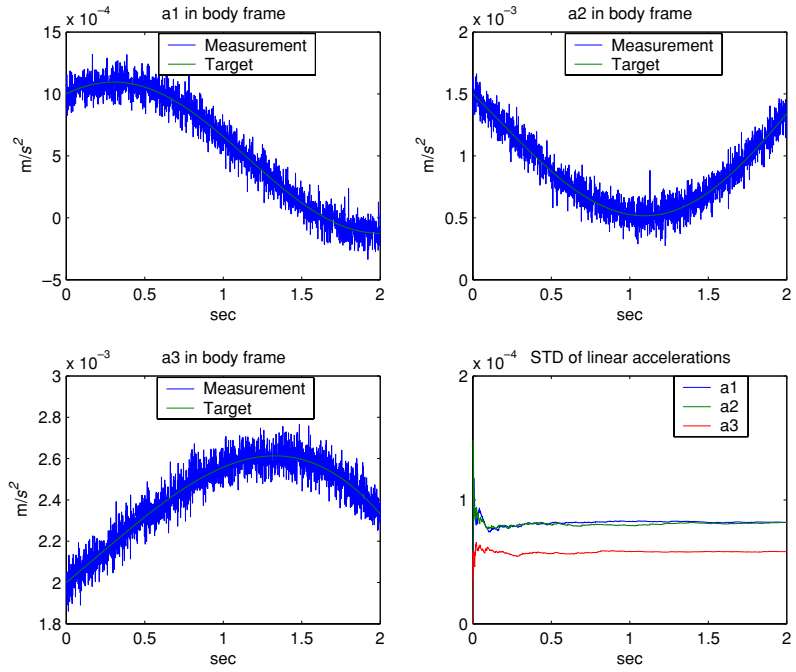

Figure 7. Linear accelerations represented in the body frame converge to their designated values.

incorporated noise the same. We found that the EKF algorithm fails to track the designated trajectories at about 2° s^{-1} and linear acceleration fails simultaneously. Therefore, we determine the sensing resolution for the system is 2° s^{-1} for the angular velocity and 10 μg for the linear acceleration. The EKF algorithm fails to identify the slow angular motion due to the fact that the resulting accelerometer measurements are even smaller than the magnitude of the noise present in accelerometer measurements. This simulation outcome corresponds to the sensing resolution predicted by the following simple relation between linear acceleration and angular velocity: $A \equiv r w^2$, where A is the linear acceleration, r is the radius of the measurement unit and w is the angular velocity. From this equation, we obtain the sensing resolution for angular velocity $\approx 2.5^\circ$ s^{-1} for the same design. As suggested by this simple relation, increasing the size of the measurement unit is one effective way to improve the sensing resolution of angular velocity.

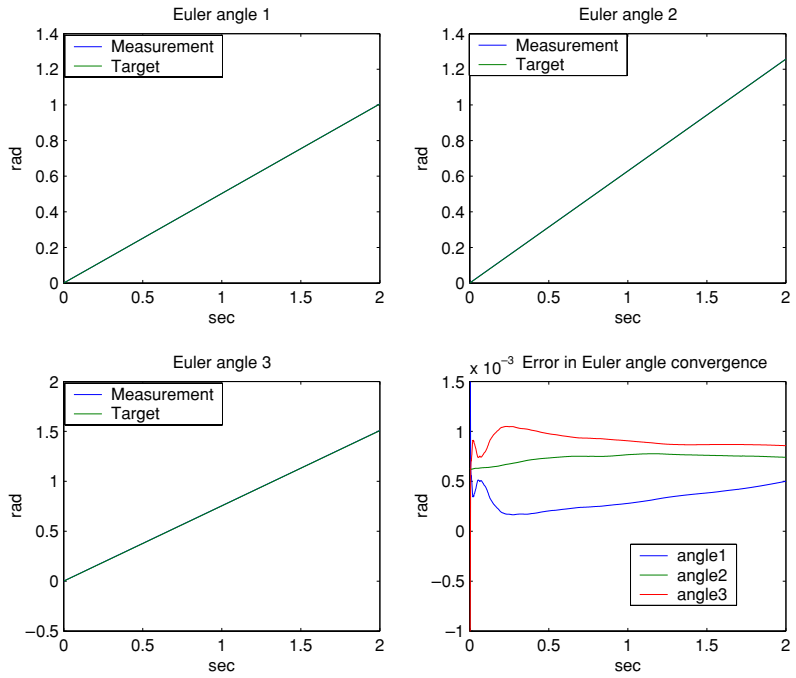

Figure 8. Euler angles converge to their designated values.

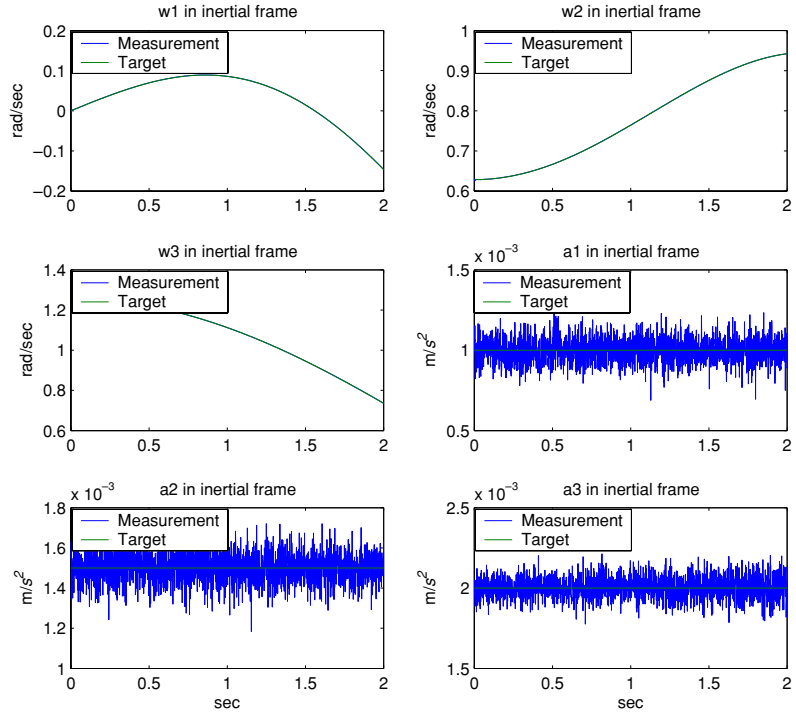

Figure 9. Angular velocities and linear accelerations, represented in the inertial frame, converge to their designated values.

4.4. Possible applications

Currently, there are various types of inertial sensors deployed in cars to facilitate advanced functionalities including: active suspension, air bag, anti-lock brakes, anti-skid system, etc [9]. The inertial sensors qualified for those applications are usually classified as automotive-grade inertial sensors and their sensing resolutions are in the range of 10–100 mg for acceleration measurement and 0.1–1° s^{-1} for angular rate measurement [18]. Our tentative IMU design has a sensing resolution roughly within this range and could be tailored to meet these performance requirements.

Due to the complexity of the car dynamics, most of the car functionalities require multiple inertial sensors to accomplish one task; meanwhile one kind of inertial sensor can be found in various functionality units simultaneously. Let us take an

Table 2. The dynamic response of a car maneuvering.

	Longitudinal acceleration	Lateral acceleration	Vertical acceleration	Yaw rate	Roll rate
Range	$\pm 50g$	$\pm 3g$	$\pm 5g$	$\pm 100^\circ\ s^{-1}$	$\pm 300^\circ\ s^{-1}$

example of a car that is equipped with rollover prevention [19] and yaw stability [20] systems: the rollover prevention sub-system utilizes four inertial sensors to measure lateral acceleration, vertical acceleration and roll rate, and the yaw stability sub-system utilizes two inertial sensors to measure lateral acceleration and yaw rate. Therefore, at least one of the lateral acceleration sensors is redundant in this case. As motivated by this example, we expect that the proposed IMU would have a great use along the development of advanced car systems in future. The proposed IMU can replace multiple sensors existing in a car nowadays and perform the integrated measurement for the six DOF motions of a car to enable multiple advanced functionalities.

The dynamic performance of a car maneuvering is listed in table 2 for [9, 18–20].

5. Conclusions

This paper presents a novel design of coplanar gyro-free IMU that consists of seven to nine single-axis accelerometers, and combined with the iterative EKF algorithm, it can be utilized to perform the six DOF measurements for an object in motion. The main advantages of this design over other gyro-free IMU designs are: (1) the outputs of the proposed gyro-free IMU are three angular velocities (in pitch, yaw, roll directions) and three linear accelerations (in the X, Y and Z directions). As a consequence, the subsequent signal processing can use less integral operation and thus can alleviate the drifting problem. (2) The single-axis accelerometers employed in the proposed IMU system are all situated on the same plane. Therefore, they can be *in situ* fabricated by micro fabrication techniques. The fabrication and assembly cost are greatly reduced. In addition to those advantages, we also show that the minimum number of single-axis accelerometers needed in the coplanar gyro-free IMU is 7–9, depending on the content of the angular velocity to be measured. Nine single-axis, linear accelerometers are needed when the angular velocities to be measured are constant. The iterative EKF state estimation algorithm is a suitable state-estimation algorithm in this design and it can successfully track down the angular velocities as well as improve sensing accuracy when the accelerometer measurements are contaminated by noise. The angular velocity sensing resolution is dictated by the sensing resolution of employed accelerometers as well as the size of the measurement unit. In a design example, we show that the sensing resolution is $2^\circ\ s^{-1}$ for the angular velocity and 10 μg for the linear acceleration when nine single-axis accelerometers, each with 10 μg sensing resolution, are deployed on a 4 inch diameter disc. Also, with help from the iterative EKF algorithm, the angle estimation error is 10^{-3} deg after 2 s.

Appendix A. The stability of the coplanar, gyro-free IMU system

The governing equation of a gyro-free IMU is stated in equation (6). With the coplanar configuration, the governing equation can be simplified as follows,

$$\begin{bmatrix} {}^b\dot{w}_1 \\ {}^b\dot{w}_2 \\ {}^b\dot{w}_3 \end{bmatrix} = (J^T J)^{-1} J^T (1:3,:) \begin{bmatrix} A_1 \\ \vdots \\ A_m \end{bmatrix} + \begin{bmatrix} {}^b w_2\, {}^b w_3 \\ -{}^b w_1\, {}^b w_3 \\ c_1\, {}^b w_1^2 + c_2\, {}^b w_2^2 + (c_1 + c_2)\, {}^b w_3^2 + c_3\, {}^b w_1\, {}^b w_2 \end{bmatrix} \tag{A.1}$$

where c_1, c_2, c_3 are determined by the location and sensing direction of the employed system-accelerometers. After linearizing at an equilibrium point, the equation above can be written as follows,

$$\begin{bmatrix} \delta\dot{w}_1 \\ \delta\dot{w}_2 \\ \delta\dot{w}_3 \end{bmatrix} = \begin{bmatrix} 0 & w_{3o} & w_{2o} \\ -w_{3o} & 0 & -w_{1o} \\ 2c_1 w_{1o} + c_3 w_{2o} & 2c_2 w_{2o} + c_3 w_{1o} & 2c_1 w_{3o} + 2c_2 w_{3o} \end{bmatrix} \times \begin{bmatrix} \delta w_1 \\ \delta w_2 \\ \delta w_3 \end{bmatrix} + \text{HOT}, \tag{A.2}$$

where the upper script b is ignored for the representation clarity. The characteristic equation related to the above state matrix is

$$\lambda^3 + \lambda^2(-2(c_1 + c_2)w_{3o}) + \cdots. \tag{A.3}$$

As shown in (A.3), the coefficient of the second term would vary with different equilibrium points, no matter how we chose the accelerometer configuration. Therefore, the stability of the coplanar, gyro-free IMU system depends on the angular velocities to be measured.

Appendix B. Sensing direction of the observer-accelerometer

According to equation (3), any out-of-plane sensing accelerometer, located at $(x, y, z) = (r_{ix}, r_{iy}, 0)$, would have the output of the following:

$$A_j = [r_{jy} \quad r_{jx} \quad 0 \quad 0 \quad 0 \quad 1] = \begin{bmatrix} \dot{w} \\ F_o \end{bmatrix} + w^T \begin{bmatrix} 0 & 0 & r_{jx} \\ 0 & 0 & r_{jy} \\ 0 & 0 & 0 \end{bmatrix} w$$
$$= J(j,:) \begin{bmatrix} \dot{w} \\ F_o \end{bmatrix} + w^T \Omega_j w. \tag{B.1}$$

Let the outputs of three system-accelerometers, which perform the out-of-plane sensing, be denoted as A_i, A_{i+1}, A_{i+2} and their respective row vectors in the J matrix be $J(i,:)$, $J(i+1,:)$, $J(i+2,:)$. Since the out-of-plane sensing accelerometers can

provide, at most, three linearly independent row vectors for the J matrix, any other out-of-plane sensing accelerometer, A_o, can have its related $J(o,:)$ represented as a linear combination of the previous three row vectors in J.

$$\begin{aligned} A_o &= J(o,:)\begin{bmatrix}\dot{w}\\ F_o\end{bmatrix} + w^T\Omega_o w \\ &= \left(J^T(i:i+2,:)\begin{bmatrix}\alpha_1\\ \alpha_2\\ \alpha_3\end{bmatrix}\right)^T\begin{bmatrix}\dot{w}\\ F_o\end{bmatrix} + w^T\Omega_o w \\ \begin{bmatrix}\alpha_1\\ \alpha_2\\ \alpha_3\end{bmatrix} &= (J(i:i+2,:)J^T(i:i+2,:))^{-1}J(i:i+2,:)J^T(o,:) \end{aligned} \tag{B.2}$$

After cranking in the relations of α_i in (B.2) into (B.1), the output of out-of-plane sensing accelerometer, other than system-accelerometers, becomes

$$A_o = \alpha_1 A_i + \alpha_2 A_{i+1} + \alpha_3 A_{i+2}. \tag{B.3}$$

The angular velocity terms disappeared in (B.3) as compared to equation (7). This implies that the observer-accelerometers must be in-plane sensing accelerometers.

References

[1] Kuo S-P, Boutelle J and Lawdermilt L 2000 Accelerometer input axis angular acceleration sensitivity *Position Location and Navigation Symposium* pp 449–56

[2] Randle J-S and Horton M-A 1997 Low cost navigation using micro-machined technology *IEEE Conf. on Intelligent Transportation System ITSC 97* pp 1064–7

[3] Luinge H-J, Veltink P-H and Baten C-T-M 1999 Estimation of orientation with gyroscopes and accelerometers *Proc. BMES/EMBS Conf. Serving Humanity, Advancing Technology* pp 884

[4] Liu J, Shi Y and Zhang W 2004 Micro inertial measurement unit based integrated velocity strapdown testing system *Sensors Actuators* A **112** 44–8

[5] Schuler A-R 1967 Measuring rotational motion with linear accelerometers *IEEE Trans. Aerosp. Electron Syst.* **3** 465–71

[6] Tan C-W, Park S, Mostov K and Varaiya P 2001 Design of gyroscope-free navigation systems *IEEE 4th Int. Conf. on Intelligent Transportation Systems* pp 286–91

[7] Wang Q, Ding M and Zhao P 2003 A new scheme of non-gyro inertial measurement unit for estimating angular velocity *Industrial Electronics Society IECON '03* vol 2 pp 1564–7

[8] Kim A and Golnaraghi M-F 2004 A quaternion-based orientation estimation algorithm using an inertial measurement unit *Position Location and Navigation Symposium PLANS 2004* pp 268–72

[9] Mostov K, Soloviev A and Koo T-K 1997 Accelerometer based gyro-free multi-sensor generic inertial device for automotive applications *ITSC 97: Intelligent Transportation System (9–12 Nov. 1997)* pp 1047–52

[10] Foxlin E, Harrington M and Altshuler Y 1998 Miniature 6-DOF inertial system for tracking HMDs *SPIE AeroSense* **3362** 1–15

[11] Yazdi N, Anazi F and Najafi K 1998 Micromachined inertial sensors *Proc. IEEE* **86** 1640–59

[12] Chen C-T 1984 *Linear System Theory and Design* (Library of Congress Cataloging in Publication Data) pp 168–227

[13] Hermann R and Krener A-J 1977 Nonlinear controllability and observability *IEEE Trans. Autom. Control* **22** 728–40

[14] Misawa E-A and Herdrick J-K 1989 Nonlinear observers—a state-of-the-art survey *Trans. ASME* **111** 344–52

[15] Cho Y-M and Rajamani R 1997 A systematic approach to adaptive observer synthesis for nonlinear systems *IEEE Trans. Autom. Control* **42** 534–7

[16] Slotine J-J-E, Hedrick J-K and Misawa E-A 1987 On sliding observers for nonlinear systems *J. Dyn. Syst. Meas. Control* **109** 245–52

[17] Bar-Shalom Y, Li X-R and Kirubarajan T 2001 *Estimation with Applications to Tracking and Navigation* (New York: Wiley) p 371

[18] Madni A, Costlow L and Knowles S 2003 Common design techniques for BEI gyrochip quartz rate sensors for both automotive and aerospace/defense markets *IEEE Sensors J.* **3** 569–78

[19] Schubert P-J, Nichols D, Wallner E-J, Kong H and Schiffmann J-K 2004 Electronics and algorithms for rollover sensing *SAE International Technical Paper* 2004-01-0343

[20] Wang Y and Nagai M 1996 Integrated control of four-wheel-steer and yaw moment to improve dynamic stability margin *Conf. on Decision and Control* pp 1783–4